Haiteng Ma[1]
School of Mechanical Engineering,
Shanghai Jiao Tong University,
Shanghai 200240, China
e-mail: haiteng.ma@sjtu.edu.cn

Wei Zeng
School of Mechanical Engineering,
Shanghai Jiao Tong University,
Shanghai 200240, China
e-mail: 020020910172@sjtu.edu.cn

Hongmei Jiang
UM-SJTU Joint Institute,
Shanghai Jiao Tong University,
Shanghai 200240, China
e-mail: jiang_plum@sjtu.edu.cn

Jun Hong
Shanghai Electrical-Mechanical
Engineering Institute,
Shanghai 201111, China
e-mail: BAbuYYB@163.com

Impact of Cooling Injection on Shock Wave Over a Flat Tip in High Pressure Turbine

Cooling design of highly loaded turbine blade tips is challenged by the scarcity of experimental data and the lack of physical understanding in cooling and overtip leakage (OTL) interaction under transonic conditions. To address these issues, this paper carried out transient thermal measurements through infrared thermography on a transonic flat tip with and without cooling injection. Experimental data of Nusselt number and cooling effectiveness were obtained and compared with computational fluid dynamics (CFD) results for numerical validation. Both experimental data and simulation results show that cooling injection drastically augments tip Nusselt number near pressure side (PS) which is upstream of ejection, and in areas around coolant holes. Moreover, a strikingly low Nusselt number stripe is observed downstream of cooling injection from one of the holes in aft portion of blade. The strip is directed transverse to local OTL streamline flowing from pressure to suction side (SS) and sprawls to adjacent coolant wakes. Further numerical analyses concluded that cooling injection changes tip aerodynamics and overtip shock wave structure fundamentally. Oblique shock waves across the uncooled flat tip are replaced by a confined shock train downstream of cooling injection and between cooling holes, which is constituted by two shocks normal to local OTL flow coming from pressure side. Across the first shock, density and pressure increases abruptly, contributing to thickening of tip boundary layer and the plummet of skin friction on tip surface, which is responsible for the sharp decline of tip Nusselt number and therefore, formation of low heat transfer stripe downstream cooling injection. [DOI: 10.1115/1.4052135]

Keywords: turbine blade, tip leakage flow, heat transfer, film cooling, shock wave

1 Introduction

High-pressure turbine (HPT) rotor blade tip is the most vulnerable part among aero-engine components, because it has the highest thermal load compared with other surfaces of turbine blade [1]. In addition, overtip leakage (OTL) flow through tip clearance of rotor blade is responsible for about 1/3 of aerodynamic efficiency loss in a turbine stage [2]. Therefore, cooling and sealing design of turbine blade tip are crucial to improve the efficiency and service life of gas turbines and are challenging due to the complexity in OTL flow and its interaction with tip cooling injection.

Classical blade tip design philosophy is partly based on experimental studies of flat tip aero-thermodynamics implemented in subsonic or low-speed wind tunnel. Denton [2] proposed that OTL flow is driven into tip clearance by pressure difference between pressure side (PS) and suction side (SS) of turbine blade. It separates at PS edge after entering tip gap and forms a vena contracta. The highest heat transfer rate is spotted at flow reattachment region [3,4]. High heat transfer is also observed in the aft portion of blade and blade leading edge, whereas a low heat transfer region resides in the thickest part of blade, entitled "central sweet spot" [5].

Cooling design of blade tips heavily relies on testing and experience [6,7], because its performance is influenced by many factors (flow condition, configuration of holes, and blade tips) in a coupled manner and physics governing of coolant/mainstream mixing is quite sophisticated [1]. For flat tip cooling, profuse experimental data have been presented in subsonic linear cascade decades ago. Film cooling effectiveness and heat transfer coefficient (HTC) were measured under various blowing ratios and tip clearances [8,9], as well as for different hole locations [10].

In highly loaded turbine stage such as single stage HPT, flow can become transonic [11,12], particularly in blade tip clearance [13,14]. Transonic features including shock wave and flow choking qualitatively alter OTL flow pattern, and even compromise classical tip design wisdom established in subsonic flow experiments. Wheeler et al. [14] demonstrated the existence of oblique shock waves within tip clearance, which result in large changes of tip boundary layer development. Oblique shock waves interact strongly with boundary layer on the casing and tip, leaving clear signature of heat transfer stripes [15,16]. In rear part of blade tip where OTL flow is supersonic, heat transfer is notably lower than that near leading edge where leakage flow is subsonic, which is different from the conclusion of Bunker et al. [5]. Furthermore, Zhang and He [17] showed local choking in transonic tip blocks the influence of suction side exit on OTL flow, resulting in breakdown of the pressure-driven mechanism established in subsonic wind tunnel. Therefore, tip design wisdoms need to be re-examined by incorporating transonic features, especially shock wave and flow choking phenomena.

Experimental data on transonic blade tip cooling, however, are quite scarce and emerge only in recent years. For transonic squealer tip cooling, Ma et al. [18] presented the first of the kind experimental heat transfer data and found distinct stripes in HTC. Saul et al. [19] and Vieira et al. [20] studied the effect of tip gap, coolant mass flowrate, and cavity welding beads on squealer tip heat load. Thermal measurement of cooled winglet tip at transonic conditions was presented by O'Dowd et al. [21]. To the best of the authors' knowledge, no experimental data of transonic flat tip cooling have been reported in open literature.

It should be noted that although flat tip incurs higher aerodynamic loss and is more susceptible to damage during rotor-casing rubbing than the squealer tip, it has no extended surface to cool so its cooling design is very simple and is still used in some turbine products [7]. In addition, flat tip is the baseline for

[1]Corresponding author.

Contributed by the Heat Transfer Division of ASME for publication in the JOURNAL OF TURBOMACHINERY. Manuscript received February 10, 2021; final manuscript received August 9, 2021; published online September 21, 2021. Assoc. Editor: Giovanna Barigozzi.

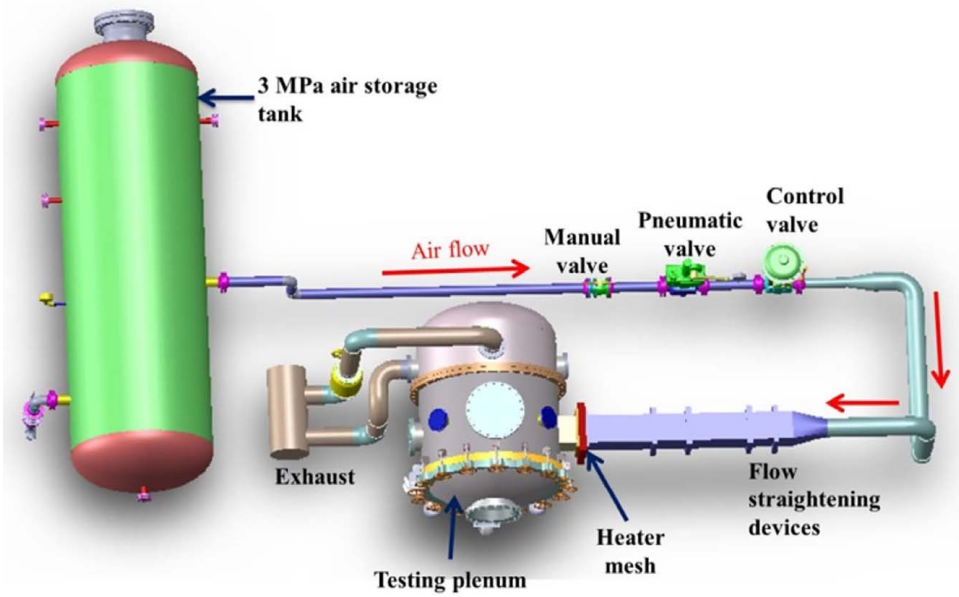

Fig. 1 Schematic of transonic wind tunnel facility [18]

understanding the complicated aerothermal mechanisms associated with OTL flow [22]. Furthermore, recent studies consistently demonstrate that coolant blowing offers more benefit for flat tip than cavity tip, especially at small tip gap. Hence, flat tip with coolant injection has the potential to seal rotor tip clearance effectively. Zhou and Hodson [23] reported tip cooling injection reduces losses for flat tips, especially when tip clearance is small, but has less influence for squealer tips. Similar conclusion was also drawn in Ref. [24], who stated total pressure loss can be reduced by 20% for a flat tip with a jet mass flowrate of 0.4% of main flow through the passage. For transonic blade tips, Wheeler and Saleh [25] found that flat tip outperforms cavity tip in terms of blade loss and turning at cooling mass flows above 2% of the mainstream. Wang et al. [26] proposed a partial squealer tip, with flat tip in rear part of blade where OTL flow is transonic. It exhibits the same aerodynamic loss as a full squealer tip, but improved design space for internal cooling. In a word, flat tip cooling is worth examining due to its simplicity in structure and cooling design, as well as its application prospect in tip sealing.

Cooling injection could influence or interact with OTL flow strongly, given that tip clearance is a confined space. This is substantiated recently by Ma et al. [27] on a transonic squealer tip through a combined experimental and numerical effort. It is found that tip aerodynamics is changed significantly by cooling injection, even in areas far away from ejection holes. OTL flow impinges on cavity floor due to squeezing of cooling counter-rotating vortex pairs (CRVPs), contributing to unique thermal stripes whose heat transfer coefficient is over 50% larger than the uncooled tip. In earlier studies, Krishnababu et al. [28] and Naik et al. [29] reported blockage effect from cooling injection decreases leakage flowrate. It also improves the under-turning of leakage flow, as presented in Refs. [30,31]. So tip leakage vortex gets smaller and loss in turbine passage is reduced [10,32].

Interaction between shock wave and film cooling has been studied on transonic airfoils by some researchers, but the conclusions are somewhat conflicting. Xue et al. [33] reported film cooling effectiveness and heat transfer coefficient on blade suction side reduce abruptly downstream of the impinging shock originated from trailing edge of adjacent blade. However, film cooling effectiveness is affected little by the impingement of trailing edge shock, as measured in annular cascade and double-passage linear cascade [34,35]. In an earlier study on flat plate, Ligrani et al. [36] stated film effectiveness is enhanced downstream of oblique shock, due to deflection of the film toward the wall. These contradictory claims are probably caused by the ad hoc nature of aforementioned studies and the dependency of shock-film cooling interaction on many factors, such as blowing ratio and airfoil shape. For turbine blade tip, interaction between cooling and overtip shock wave within the confined tip gap is expected to be more sophisticated, yet relevant physical investigation has, to the best of the authors' knowledge, never been carried out before.

To address these challenges, this paper presents the first of the kind experimental heat transfer data on a transonic cooled flat tip, based on which the impact of cooling injection on overtip shock wave structure and thermal signature is illuminated. Transient thermal measurements using infrared thermography were carried out on a transonic flat tip with and without cooling, in a linear cascade whose exit Mach and Reynolds number are 0.95 and 0.88×10^6, respectively. Numerical simulations were also implemented, whose sensitivity to mesh and turbulence models is thoroughly tested. Experimental data on tip Nusselt number and cooling effectiveness were obtained and compared with computational results for validation purposes. Several unique thermal features are observed consistently in experimental and numerical results. In particular, a distinct low heat transfer stripe exists on tip surface, located downstream of cooling injection in transonic part of blade and directed transverse to local OTL flow streamline, indicating the signature of shock wave. Finally, aerothermal interaction mechanism behind these features are analyzed using numerical approaches, with a focus on the impact of cooling injection on overtip shock wave structure, as well as its connection to tip heat transfer characteristics established through the combined experimental and numerical effort.

2 Experimental Setup and Methodology

Experiments in present study were conducted on the transonic blow-down wind tunnel at Aero-Thermal Lab, Shanghai Jiao Tong University. As schematized in Fig. 1, compressed air is stored in a 10 m^3 tank (allowable pressure is 3 MPa) and released through a series of valves. To adjust total pressure at the inlet of test section, a Fisher valve (EWT Body with 667 actuator and Fieldvue DVC6000 controller) controlled through an extended Karman filter algorithm as described in Refs. [37,38] was used. Airflow is homogenized by honeycomb screens and flow straightening

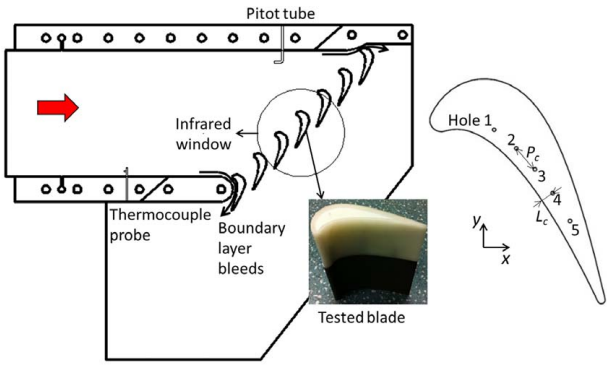

Fig. 2 High-speed linear cascade and test blade with flat tip cooling holes

devices and heated by a fine mesh (aperture size of 0.08 mm and filament diameter of 0.05 mm) powered by a 100 kW DC supply. This wind tunnel has been a platform for several transonic blade tip experiments previously, including Refs. [18,39,40].

Figure 2 shows the high-speed linear cascade and configuration of cooled flat tip. Periodicity of the test section is ensured by using seven blades and bleeding boundary layer fluid on two sidewalls. The test blade, which is situated in the center of the linear cascade, is composed of two parts. The upper part is made from resin (DSM Somos 14120) by stereolithography, whose thermal conductivity is about 0.2 W/m-K at room temperature. Heat penetration depth is calculated to be 1.5 mm at 2 s, which is far below the height of upper blade (28 mm). So heat transfer within the upper blade can be modelled as transient conduction in a one-dimensional semi-infinite solid. Geometric parameters of the blade and tip cooling holes are listed in Table 1. Tip clearance (g) is 0.675 mm and about 1% of blade span (S). For the cooled case, five holes with a diameter (D) of 0.8 mm and an injection angle of 90 deg are arranged on tip surface in middle and aft portion of blade where the baseline OTL flow in uncooled case is supersonic.

Table 1 Geometry of turbine blade and tip cooling holes

Blade	Flow inlet angle, α (deg)	45.3
	Axial chord, C_x (mm)	38.99
	Pitch, P (mm)	48.2
	Tip gap height, g (mm)	0.675
	Span, engine-equivalent, S (mm)	69.5
Cooling	Diameter, D (mm)	0.8
	Pitch, P_c (mm)	6.4
	Injection angle (deg)	90
	Distance from PS edge, L_c (mm)	2.8

The five holes are placed at a distance of 3.5D from the PS edge, with a pitch (P_c) of 8D.

Figure 3 schematizes test section and coolant feed system. Mainstream pressure and temperature are measured by Pitot tube and thermocouple (K-type, Omega Engineering) at cascade inlet. Coolant is extracted from air storage tank through a pressure regulating valve. The core elements are vortex tubes which can produce a nearly 15 K temperature drop at the cold end. The cold air is measured by a flowmeter for volumetric flowrate and then homogenized in thermally insulated setting chamber, where its total pressure and temperature are measured. It is then buffered within the hollow in upper blade, before ejecting into tip gap.

Flow conditions for present transonic turbine cascade experiment are listed in Table 2. Mach number at cascade exit is 0.95, so cascade flow is transonic especially at tip gap region. Total pressure of coolant is controlled to be 1.1 ± 0.01 times that of cascade inlet. As a result, mass flowrate of coolant is measured to be 0.47% of that of mainstream in a single passage in engine-realistic condition. Average blowing ratio with reference to cascade exit is estimated to be 2.4. Total temperature ratio between coolant and mainstream is controlled to be 0.9 ± 0.004. Turbulent intensity at cascade inlet is around 1%.

Time history of total pressure and temperature at the inlet of cascade during a blow-down test is graphed in Fig. 4. Inlet pressure is stabilized at 180 ± 1 kPa after a valve transient of 5.5 s. Heater

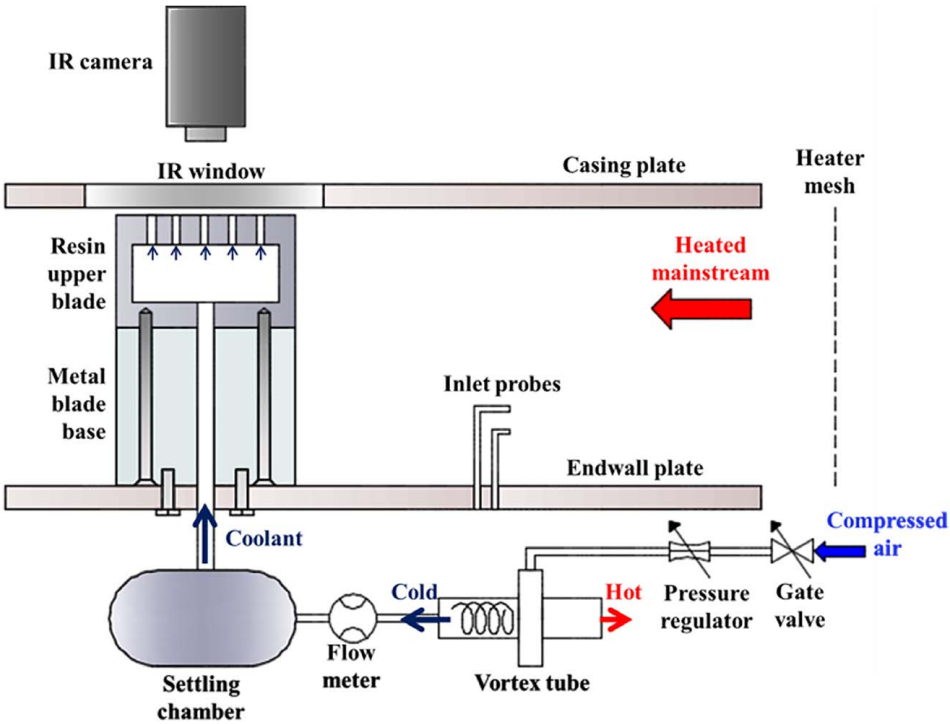

Fig. 3 Schematic of test section and coolant supply system

Table 2 Flow conditions

Inlet	Total Pressure (Pa)	180,000
	Mach	0.3
	Reynolds ($=\rho_{in}U_{in}C_x/\mu$)	0.26×10^6
Outlet	Static pressure (Pa)	101,325
	Mach	0.95
	Reynolds ($=\rho_eU_eC_x/\mu$)	0.88×10^6
Coolant	Total pressure (Pa)	198,000
Cascade mass flowrate (kg/s)		3

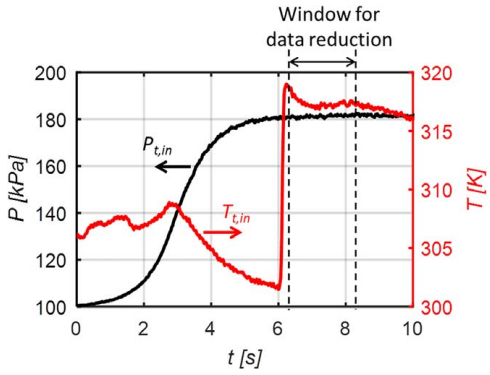

Fig. 4 Time history of total pressure and temperature at cascade inlet

mesh is then switched on to provide a step increase in mainstream temperature. Coolant feed system is precooled for 30 min to reach thermal equilibrium before each blow down. Two seconds of transient thermal measurement data immediately after heating are selected for data reduction. It is estimated that heat penetrates to a depth of 1.5 mm.

Transient thermal measurement of tip surface temperature of central blade is implemented by an infrared camera (FLIR A325, 320×240 pixels, 60 Hz). Material for infrared glass is zinc-selenide (ZnSe). To avoid large uncertainties such as surface emissivity, infrared window transmissivity associated with built-in calibration for infrared camera, one thermocouple is placed flush with the tip surface to conduct in situ calibration. Figure 5 shows the linear calibration curve between grayscale and temperature reading for infrared camera.

From time history of surface temperature, heat flux q'' can be reconstructed using the impulse method by Oldfield [41]. During the data reduction window shown in Fig. 4, convective heat transfer coefficient (HTC, h) is constant because the aerodynamics is in

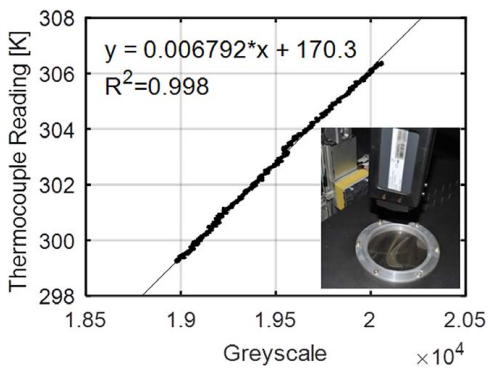

Fig. 5 Calibration for infrared camera

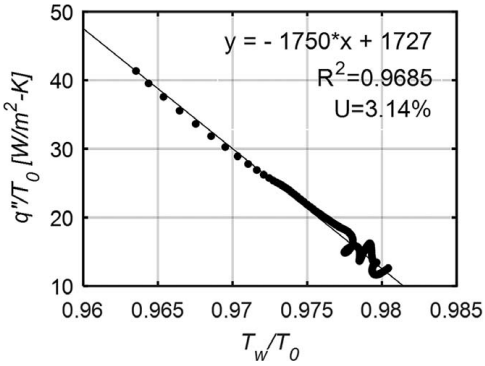

Fig. 6 Data reduction at one sample point

steady state. According to Newton's law of cooling

$$q'' = h(T_{ad} - T_w) \tag{1}$$

When mainstream total temperature (T_t) is constant

$$\frac{q''}{T_t} = -h\cdot\frac{T_w}{T_t} + \frac{hT_{ad}}{T_t} \tag{2}$$

For the cooled case, adiabatic temperature $T_{ad,c}$ is dependent on both mainstream and coolant temperature and is constant during the data reduction window shown in Fig. 4. For the uncooled case, adiabatic temperature $T_{ad,uc}$ is proportional to mainstream total temperature [42,43], and a ramp heating method was developed by Ma et al. [39] to reduced transient thermal measurement uncertainty. Finally, h and T_{ad} are derived from linear regression between heat flux and wall temperature. To nondimensionalize heat transfer coefficient, a characteristic length of *2 g* is selected, based on the reasoning elaborated in Sec. 5.2, and the Nusselt number is defined as $\mathrm{Nu}=2hg/k$.

Linear regression procedure is illustrated in Fig. 6 for one sample point on tip surface. Coefficient of determination (R^2) is 0.9685 and relative uncertainty in linear regression with 95% confidence ($\%U$) is 3.14%. On the whole tip surface, linear regression goodness is also acceptable with an uncertainty level below 10%, as contoured in Fig. 7. Regression performance is relatively poor in areas with low HTC, because the smaller wall temperature rise leads to lower signal-to-noise ratio.

Uncertainty in transient thermal measurement is listed in Table 3. Thermocouple uncertainty is scaled by the overall temperature difference in heat transfer experiment, which is 30 K. Through four repeated runs, the average uncertainty level in heat transfer coefficient and cooling effectiveness is ±8.7% and ±13.2%, respectively, which is commensurate with that typically reported in literature [8,21]. It should be noted that in the region covered by coolant wakes, cooling effectiveness is around 0.5, so its uncertainty is

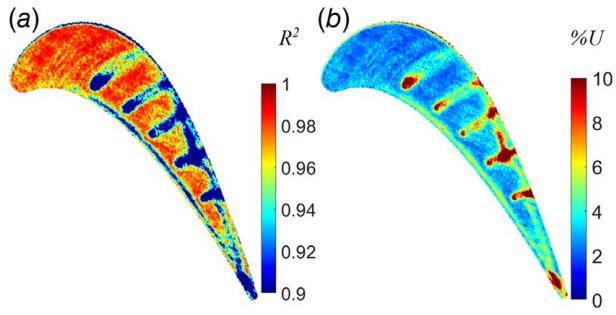

Fig. 7 Contours of linear regression uncertainty on cooled flat tip from a single run: (*a*) coefficient of determination and (*b*) regression uncertainty

Table 3 Uncertainty level in measurements

Measured quantity	Uncertainty (95% C)
Wall temperature (T_w)	4% (30 ± 1.2 K)
Inlet temperature (T_{in})	4% (30 ± 1.2 K)
Nusselt number (Nu)	±8.7%
Cooling effectiveness (η)	±13.2%

comparatively small (±0.025, or ±5%). But in the region unprotected by the coolant, cooling effectiveness can be as low as 0, so its relative uncertainty has a large percentage (beyond ±15%).

3 Computational Setup and Sensitivity

Numerical domain is a single blade passage with periodic boundary condition on lateral sides. Only feed pipes are modelled for coolant system. Boundary conditions are specified to match the cascade mass flowrate, exit pressure and ratios of total pressure and temperature between coolant and cascade inlet in experiments. Total pressure and temperature at cascade inlet are specified as 2.0 bar and 318 K, and those at cooling pipe inlet are designated as 2.2 bar and 288 K. Static pressure at cascade outlet is specified as 1.0 bar. Turbulent intensity at inlet boundary is 1%, which is commensurate with the experimental measurement. Symmetry is imposed on the hub. On blade and tip surfaces, two isothermal wall boundary conditions ($T_w = 268/278$ K) are calculated, and their heat fluxes are subtracted to derive computational heat transfer coefficient. In addition, adiabatic wall boundary condition is also computed.

Computational mesh is illustrated in Fig. 8. It is a structured mesh with 12 million nodes. Minimum grid size near wall is 0.002 mm to ensure that y^+ value near wall is around 1. There are 50 grid points in the radial direction from the tip to the casing and 48 nodes on the circumference of cooling holes. Mesh independence study is carried out and relevant parameters are listed in Table 4. Average y^+ and h on tip surfaces converge with smaller increment as the mesh size increases. Figure 9 shows the relative difference of Nusselt number on tip surfaces between meshes with 12 and 15 million nodes is far below that between meshes with 8 and 12 million nodes. Therefore, mesh with 12 million nodes is adequate for the present study.

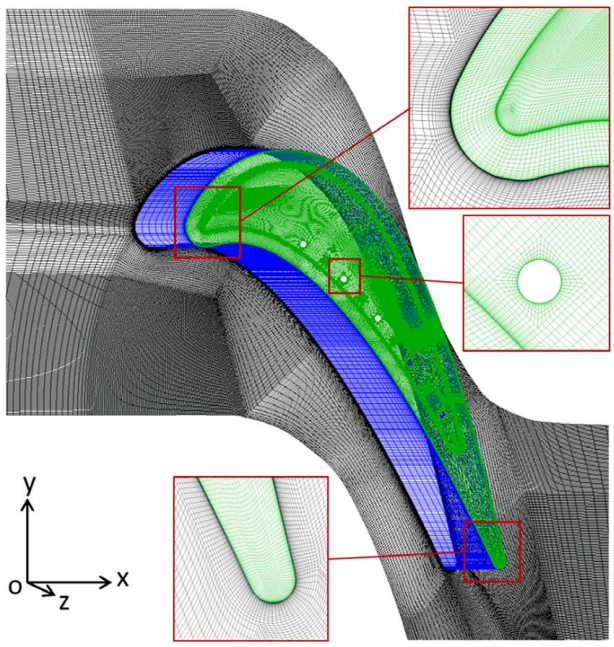

Fig. 8 Mesh topology

Table 4 Parameters in mesh dependence study

Grid size	8 million	12 million	15 million
Nodes in tip gap	30	50	70
$\overline{y^+}$ on tip	1.085	1.097	1.099
$\overline{Nu}$ on tip	81.145	82.513	82.674

Computational fluid dynamics (CFD) solver in present study is ANSYS FLUENT. It is steady, density based with implicit formulation. Second-order accuracy is selected for spatial discretization of flow and turbulence quantities. Three Reynolds-averaged Navier–Stokes (RANS) models are used and validated against experimental data in Sec. 4: Spalart-Allmaras (SA), k-ω SST, and Reynolds stress model.

4 Experimental Results and Numerical Validation

4.1 Nusselt Number. Nusselt number on the cooled flat tip obtained from transient thermal experiment and CFD with three RANS models are contoured in Fig. 10. Qualitative pattern between experimental data and RANS results shows analogous trend. High Nusselt number of above 80 is consistently observed near leading edge stagnation point, PS edge (upstream of each cooling hole), and around each cooling hole with similar patterns. Interestingly, downstream of cooling injection from the fourth hole, a strikingly low stripe of Nusselt number is noted both experimentally and numerically, as highlighted in the black box. This low Nusselt number strip is directed transverse to local OTL flow streamline (from PS to SS) and extends to adjacent cooling injection wakes. This unique thermal stripe should be a signature of overtip shock wave and will be discussed in Sec. 5 thoroughly.

Figure 11 shows circumferentially averaged Nusselt number distribution along the axial direction. Qualitative trend of experimental data is reproduced well by all three turbulence models. Nusselt number declines near leading edge and then exhibits five peaks in the middle/aft portion of the blade ($x/C_x = [0.35, 0.9]$), which relates to the high Nusselt number around each discrete injection shown in Fig. 10. Axial position of the five peaks also matches well between experiment and CFD. Quantitative deviation between experiment and three RANS models is mostly within 20% near leading edge. In middle/aft portion of the blade where the coolant is ejected ($x/C_x = [0.35, 0.9]$), discrepancy among the three RANS models is in general, much smaller than that between each of them and the experiment. All three turbulence models overpredict circumferentially averaged Nusselt number. The overestimation percentile is mostly within 50%, except in $x/C_x = [0.6, 0.8]$ where the experimental data reach the minimum. Here, quantitative deviation from experiment has a maximum level of 70–90% for three RANS models.

To calibrate the accuracy of the three RANS models in the distinct stripe of low Nusselt number, a cut line (marked as "2") is extracted in

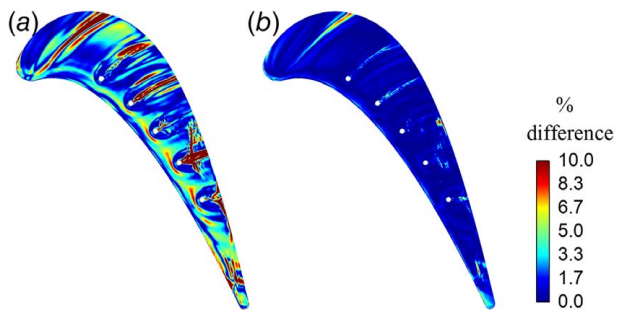

Fig. 9 Relative difference of Nusselt number between different mesh sizes: (*a*) 8 and 12 million and (*b*) 12 and 15 million

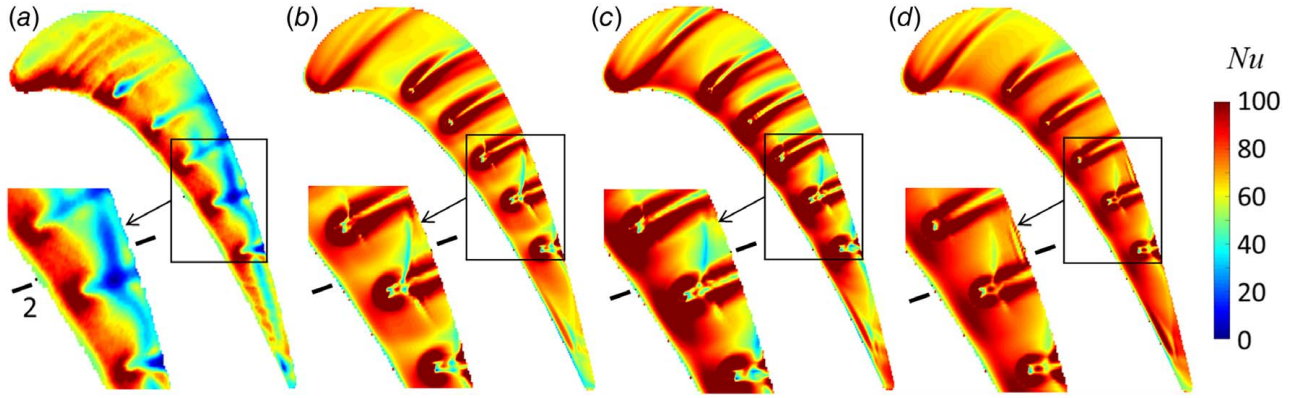

Fig. 10 Nusselt number on flat tip with cooling injection: (*a*) experiment, (*b*) SA model, (c) *k-ω* SST model, and (*d*) Reynolds stress model

Fig. 10. Nusselt number variation along this cut line is plotted in Fig. 12. Qualitative trend between experiment and three RANS models displays good accordance. Nusselt number increases after entering tip clearance from PS edge ($s/g = [0, 2.5]$), then declines monotonically to a minimum near $s/g = 9$, and is augmented abruptly thereafter. Quantitatively speaking, *k-ω* SST model shows the closest agreement with the experiment on this extracted line, which is of utmost interest to this paper. Thus, RANS with *k-ω* SST model is adopted in the CFD analyses of Sec. 5.

For the baseline case without cooling holes, contours of Nusselt number from experimental measurement and RANS simulations with three models are shown in Fig. 13. Overall qualitative trend of high Nusselt number in frontal part of blade and low Nusselt number in the rear part is captured by both experiment and RANS with SA and *k-ω* SST models. High Nusselt number originating from leading edge stagnation point is consistently seen from experimental data and RANS results with three different models. These two observations coincide with that reported in Ref. [16]. Quantitatively speaking, all three RANS models overpredict tip Nusselt number in aft portion of blade greatly, particularly in the locally high Nusselt number region near PS edge where separation bubble of OTL flow reattaches. This overprediction of tip Nusselt number near PS edge is also reported in Ref. [44].

Comparing tip Nusselt number between cooled (Fig. 10) and uncooled (Fig. 13) cases from experimental measurements and RANS computations with *k-ω* SST model, it is concluded that cooling injection alters tip Nusselt number pattern completely, indicating a dramatic change of tip aerodynamics. This further substantiates the statement of Ma et al. [27] made on a transonic squealer tip with cooling injection. Tip Nusselt number is augmented significantly by cooling injection near PS edge (upstream of cooling ejection), as well as in middle and aft portion of blade where cooling holes are drilled. Low Nusselt number region shrinks from across the rear part of blade in the uncooled case to a confined stripe between cooling injection that is directed transverse to local OTL flow streamline from PS to SS.

4.2 Cooling Effectiveness. Decrease of local driving temperature for heat transfer on the wall due to coolant ejection is evaluated by a nondimensional cooling effectiveness defined as [21]

$$\eta = \frac{T_{ad,uc} - T_{ad,c}}{T_{ad,uc} - T_{t,c}} \tag{3}$$

where $T_{ad,uc}$ and $T_{ad,c}$ are the adiabatic temperature for the uncooled and cooled case, respectively. $T_{t,c}$ stands for total temperature of coolant. Two separate test runs were conducted to obtain cooling effectiveness.

Cooling effectiveness results obtained from experiment and CFD with *k-ω* SST model are shown in Fig. 14. Qualitative pattern between experiment and CFD agrees well with each other. Downstream of each discrete hole, a strip of high cooling effectiveness exists, as a signature of the ejected coolant subject to OTL flow. Moreover, a narrow stripe of high effectiveness is spotted downstream of cooling injection from the fourth and fifth hole, respectively, which is directed transverse to local OTL flow streamline and extending to adjacent coolant wakes. This is associated with the strip of highly transonic Mach number shown in Fig. 15. According to Refs. [42,43], higher Mach number in compressible flow results in lower adiabatic temperature and hence, larger cooling effectiveness value.

In summary, CFD with *k-ω* SST model in present study can serve as a reliable tool to explore aerothermal patterns qualitatively,

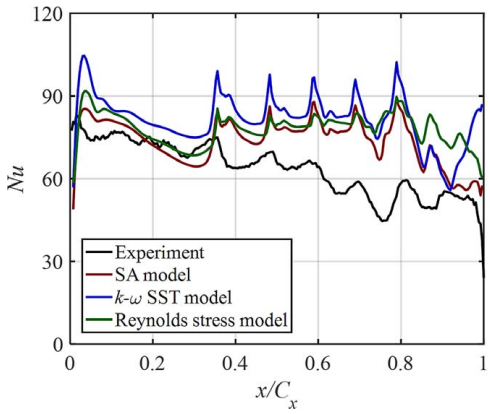

Fig. 11 Circumferentially averaged Nusselt number along axial direction for cooled flat tip

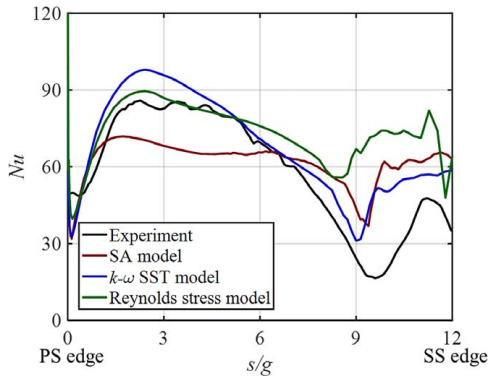

Fig. 12 Nusselt number along cut line 2 in Fig. 10

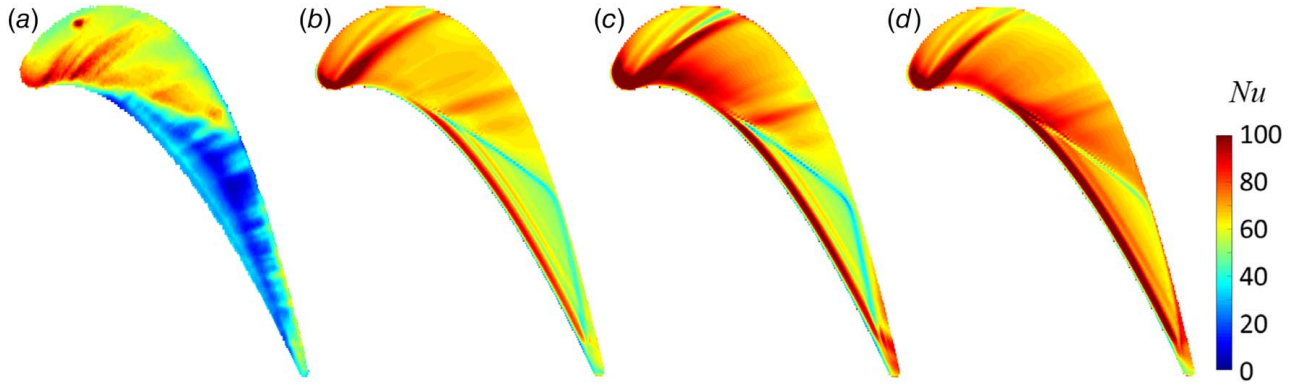

Fig. 13 Nusselt number on uncooled flat tip: (*a*) experiment, (*b*) SA model, (c) *k-ω* SST model, and (*d*) Reynolds stress model0

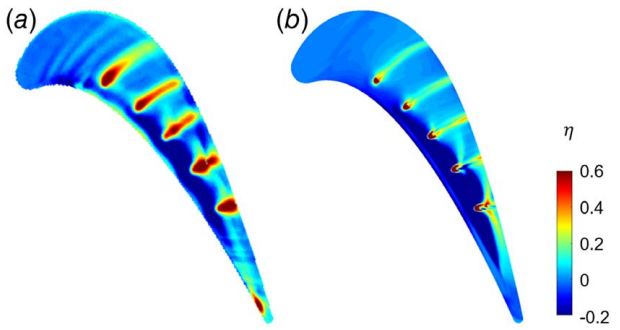

Fig. 14 Cooling effectiveness: (*a*) experiment and (*b*) CFD (*k-ω* SST)

which is the main objective of this paper. In particular, the unique stripe of low Nusselt number in cooled flat tip is captured by the numerical solver. Nonetheless, cautions are required when using the present numerical approach to gauge flow and heat transfer quantities accurately.

5 Analyses and Discussions

In this section, CFD results obtained from *k-ω* SST model, which have been validated by experimental data, are analyzed thoroughly to explore cooling injection impact on tip aerodynamics, with an emphasis on tip shock wave structure, as well as its link to tip heat transfer, particularly the unique low Nusselt number stripe transverse to local OTL flow streamline that is noted both experimentally and numerically.

5.1 Tip Leakage Aerodynamics. An overall picture of cooling injection impact on tip flow field, as represented by Mach number distribution at mid-gap, is shown in Fig. 15. For the uncooled case, OTL flow is supersonic in middle and aft portion of blade. When coolant is introduced from five discrete holes in this region, tip Mach number is changed substantially. OTL flow Mach number is reduced greatly due to the blockage effect by cooling injection, which is in concert with the findings of Ref. [45]. OTL flow becomes subsonic near PS edge, which is upstream of cooling ejection, as well as in coolant wakes. Supersonic flow exists only in areas between cooling holes and downstream of injection, as well as near trailing edge. A thin strip of highly transonic Mach number appears downstream of cooling injection from the fourth and fifth hole respectively, which corresponds to the stripe of cooling effectiveness as explained in Sec. 4.2.

Cooling injection can also influence tip aerodynamic field in regions far away from ejection holes where coolant is not supposed to reach. As shown in Fig. 15, reduction of Mach number due to cooling injection from the last hole extends toward trailing edge by around 10 diameters of cooling hole. For further demonstration, a radially extruded surface along the SS edge of blade tip is extracted in the fluid domain (whose projection is highlighted in Fig. 16), where OTL flow is supposed to exit the tip clearance. The radially

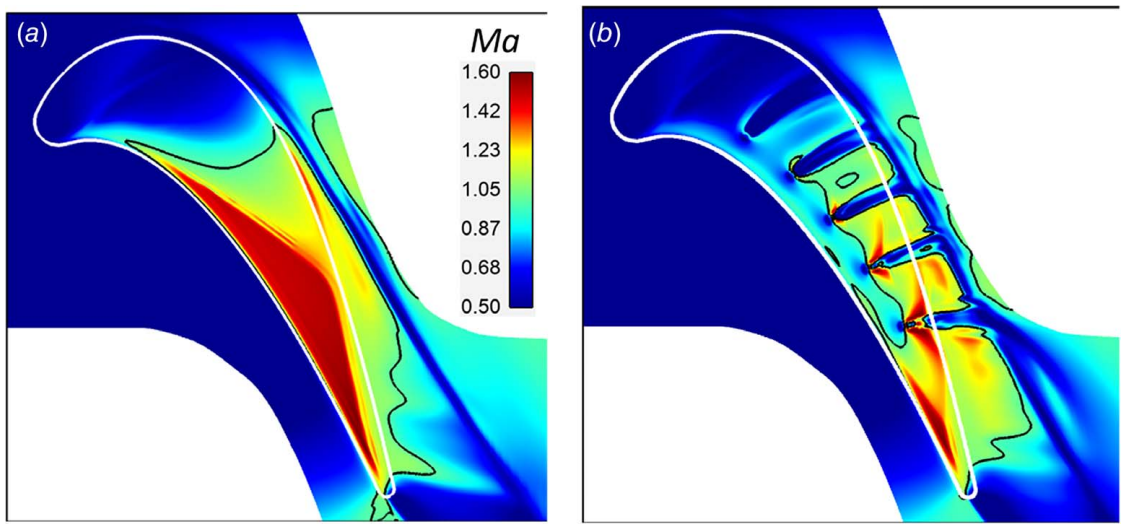

Fig. 15 Mach number at mid-gap (*z*/*g* = 0.5), with contour of Mach = 1 shown in black: (*a*) uncooled and (*b*) cooled

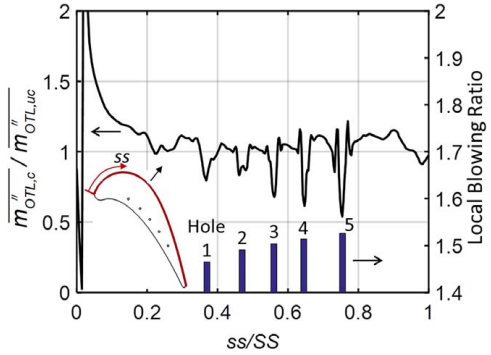

Fig. 16 Ratio of the leakage mass flux between cooled and uncooled cases along the curve length of blade SS edge (left axis), and local blowing ratio of each cooling injection (right axis)

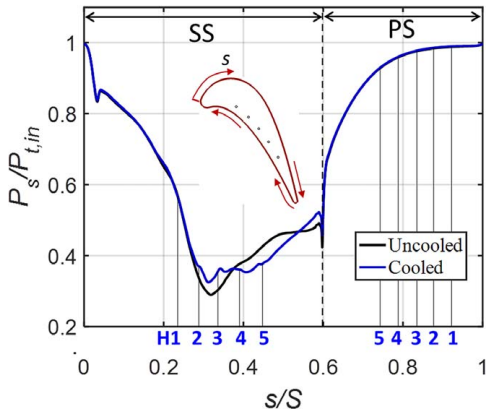

Fig. 17 Dimensionless static pressure along blade surface at 98% span (location of the five holes as projected onto PS and SS also indicated)

averaged OTL mass flux on this surface is calculated by

$$\overline{m''_{OTL}} = \left[\int_0^g (\rho \mathbf{V} \cdot \mathbf{n})\, dz\right] / g \tag{4}$$

where $\mathbf{n}$ is the unit vector normal to the extruded surface, dz is the differential element in the radial direction, where $z = 0$ corresponds to the blade tip surface and $z = g$ relates to the casing. Ratio of the radially averaged OTL mass flux between the cooled and uncooled cases is plotted in Fig. 16 against the local nondimensional curvilinear coordinate (ss/SS, where SS is the curve length of the blade SS edge). The five troughs in this graph results from the blockage effect of each discrete coolant injection, so the local leakage mass flux is reduced compared with the uncooled case. Near blade leading edge, which is distant from the first hole, leakage mass flux is augmented by more than 50%. Thus, cooling injection yields global impact on tip leakage flowrate.

Figure 16 also displays the local blowing ratio for each coolant injection, defined as the ratio of average mass flux in each cooling hole to that on the PS edge of tip clearance, where the leakage flow enters tip gap. Local blowing ratio increases monotonically from 1.46 at the first hole to 1.52 at the fifth hole, because the static pressure at the outlet of the cooling holes reduces toward trailing edge. As a result, reduction of the leakage mass flux caused by discrete cooling ejection becomes more evident at cooling holes closer to trailing edge.

Blade loading distribution at 98% span for the uncooled and cooled cases is graphed in Fig. 17, with the projected location of five cooling holes' centerlines on PS and SS also denoted. Static pressure on blade suction side surface alters notably from the second hole to trailing edge, while in other areas of blade surface, static pressure is basically unaffected by cooling injection. The lowest surface pressure is encountered at $s/S \sim 0.3$ on blade suction side, where the isentropic Mach number reaches 1.2.

5.2 Overtip Shock Wave Structure and Its Thermal Signature. To explore the underlying physical mechanism behind the markedly stripe of low Nusselt number downstream of cooling injection from the fourth hole as noted both experimentally and numerically in Sec. 4.1, six cut planes around the fourth hole are extracted as shown in Fig. 18(*a*). Cut planes 1–4 are directed normal to the camberline, with plane 3 cut through the central axis of the fourth hole. Pitchwise distance from cut plane 1, 2, and 4 to the center of the fourth hole is 4.2*D*, 2.5 *D*, and 2.0*D*, respectively, and the coolant has not spread to these planes, as will be demonstrated in Sec. 5.3. The cut line shown in Fig. 10 is actually the radial projection of cut plane 2 in Fig. 18(*a*). Tangential unit vectors of these cut planes ($\mathbf{s}$) can be regarded approximately as directed along local OTL flow streamlines from PS to SS of blade tip. Distributions of density gradient along local OTL flow streamwise direction, denoted by $\nabla\rho \cdot \mathbf{s}$, are plotted on three cut planes for the cooled and uncooled cases in Figs. 18(*b*) and 18(*c*), while blade and tip surfaces are contoured by Nusselt number. Cut plane 5 and 6 are directed tangential to the camberline, whose streamwise distance from the fourth hole's centerline is 1*D* and 3*D*. Aerothermal quantities on these two planes will be discussed in Sec. 5.3.

As demonstrated in Fig. 18, cooling injection changes overtip shock wave structure completely. For the uncooled case, oblique shock wave initiates from the separation bubble near PS edge, reflects between tip and casing walls to interact with boundary layers, and ends with multiple shocks near camberline (on cut plane 1–2) or SS edge (on cut plane 4). This pattern of oblique shock reflection has been established by Zhang et al. [16]. For the cooled case, however, the oblique shock waves no longer exist. Instead, a shock train comprised two shocks normal to the incoming OTL flow is observed. It spans a limited range in tip, originating after camberline downstream of cooling injection, and terminating through two shocks before exiting tip gap. In fact, OTL flow becomes supersonic only after camberline, as shown in Fig. 19(*b*). Near PS edge, OTL flow is subsonic due to deceleration by cooling blockage effect. Combining the distribution of OTL steamwise density gradient on cut plane 1 and 2 in Fig. 18(*b*), it is seen that the first shock in the shock train correlates well with the low Nusselt number strip of interest. Front surface of the first shock in the shock train is also directed transverse to local OTL flow streamline, similar to the low Nusselt number strip. The aerothermal link between these two will be elucidated in the following analyses on cut plane 2. Physical scenario on cut plane 1 and 4 is similar to that on cut plane 2 and will be omitted for brevity.

It is worth noting that for the uncooled flat tip of transonic turbine blade, tip leakage flow can be regarded as compressible flow in constant area ducts with friction, or so-called "Fanno flow," whose analytical solutions have been derived in the classical textbook by Shapiro [46], albeit from a simple one-dimensional point of view. Similarly, for the cooled flat tip, tip leakage flow can be modeled as the Fanno flow having the resistor of the film jet in the flow path. Thus, analyses in the following are organized with the Fanno flow between parallel plates with a gap size of g in mind. The characteristic length in this type of low is the hydraulic diameter, defined as four times the ratio of cross-sectional area to wetted perimeter, or 2 g in our case.

Figure 19 shows Mach number distribution on cut plane 2 for uncooled and cooled tips, with the contour of Mach = 1 in black. Tip Mach number is decreased significantly by cooling ejection. Near PS ($s/g = [0, 4]$), OTL flow regimes changes from supersonic to subsonic. Hence, oblique shock waves no longer exist in the cooled tip. Separation bubble on tip surface is enlarged conspicuously, owing to adverse pressure gradient as illustrated in Fig. 20(*b*). Near camberline ($s/g = [4, 8]$), OTL flow in cooled tip accelerates to supersonic regime subject to favorable pressure

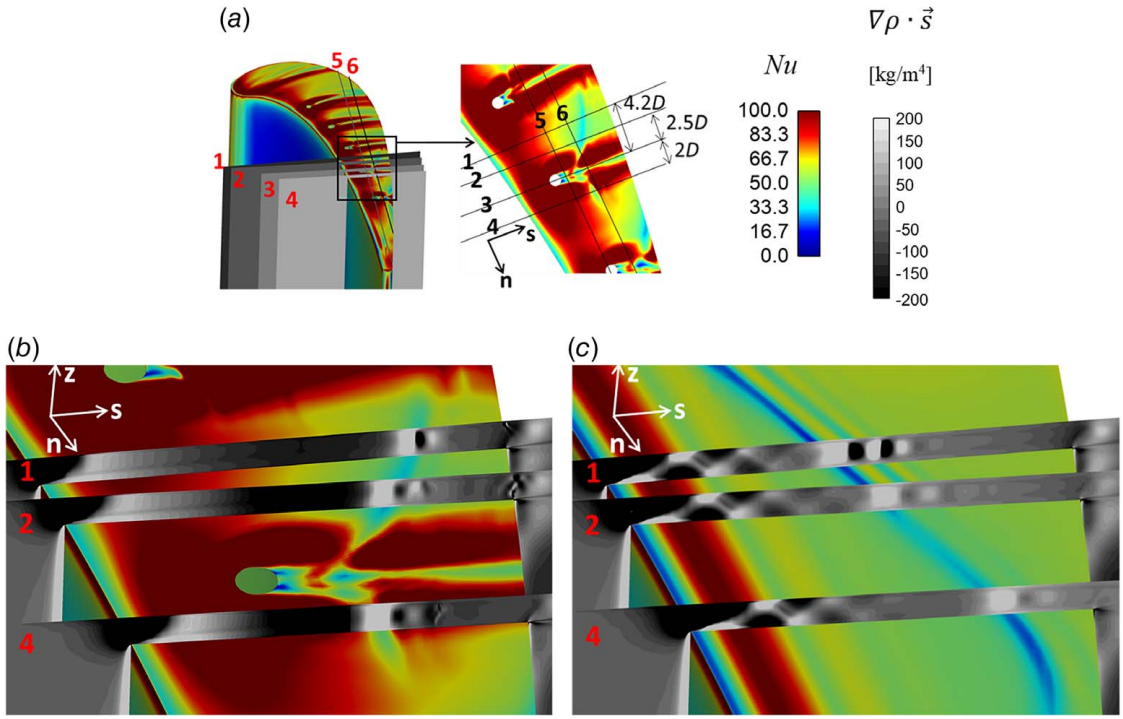

Fig. 18 Density gradient along local OTL streamwise direction on selected cut planes (blade and tip surfaces contoured by Nusselt number): (*a*) location of cut planes near the fourth cooling hole, (*b*) cooled, and (*c*) uncooled

gradient as displayed in Fig. 20(*b*). Separation bubble gradually reattaches to tip surface. At $s/g = 9$, OTL flow Mach number decreases abruptly, corresponding to the first shock in the shock train. Then OTL flow reaccelerates and decelerates again at $s/g = 10$, as a result of the second shock in the shock train. Afterward, OTL flow reaccelerates gradually to exit the tip gap. Reacceleration after each shock is a typical behavior in shock train [47] and is associated with the aerodynamic nozzle effect in the core flow [48].

Figure 20 contours static pressure nondimensionalized by cascade inlet total pressure on cut plane 2 for uncooled and cooled tips. Near PS ($s/g = [0, 4]$), tip pressure field is augmented markedly by cooling injection due to blockage effect, promoting OTL flow separation on tip surface shown in Fig. 19(*b*). Then it decreases around camberline ($s/g = [4, 8]$), contributing to the acceleration of OTL flow to supersonic regime and the reattachment of separation bubble, as described by Fig. 19(*b*). At $s/g = 9$, an abrupt rise of static pressure is manifested, which is related to the first shock in the shock train. Pressure rise across the second shock in the shock train at $s/g = 10$ is unnoticeable because it is much weaker than the first shock, as will be illustrated in Fig. 21(*b*).

To demonstrate the variation static pressure more clearly, Fig. 21 displays gradient of nondimensional static pressure along local OTL flow direction, denoted by $\nabla(P/P_{t,in})\cdot\mathbf{s}$, on cut plane 2 for uncooled and cooled tips. For the uncooled baseline case, pressure increases after each reflection foot of oblique shock waves on tip and casing walls. Between two oblique shock waves, pressure reduces due to supersonic acceleration [16]. The oblique shock waves are terminated by two shocks normal to OTL flow direction near camberline ($s/g = [7, 8.5]$), manifested by increases of streamwise static pressure.

For the cooled case, tip pressure field is characterized by adverse pressure gradient along OTL streamline near PS ($s/g = [0, 4]$), and then favorable pressure gradient near camberline ($s/g = [4, 8]$). Moreover, banded pattern of adverse pressure gradient followed by a favorable one is observed repeatedly at $s/g = 9$ and 10. Combined with streamwise density gradient contour in Fig. 18(*b*), it is concluded that the banded pattern is a manifestation of a shock train composed of two shocks normal to OTL flow from PS to SS. Pressure and density increase across each shock and reduces afterward due to reacceleration. The first shock is stronger than the second, facilitating the thickening of boundary layer on tip surface at $s/g = 9$ shown in Fig. 19(*b*).

To elaborate aerodynamic behavior of the shock train in cooled flat tip, Fig. 22 graphs the nondimensional static pressure at tip surface and mid-gap along local OTL flow direction on

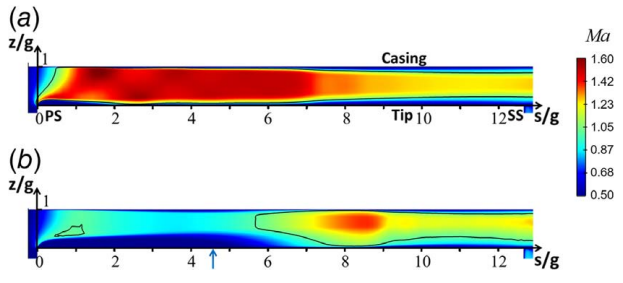

Fig. 19 Mach number on cut plane 2 (location shown in Fig. 18(*a*)), with contour of Mach = 1 in black: (*a*) uncooled and (*b*) cooled (projection of central axis of the fourth cooling hole shown in arrow)

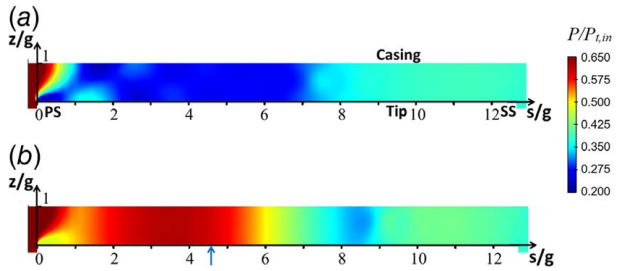

Fig. 20 Dimensionless static pressure on cut plane 2 (location shown in Fig. 18(*a*)): (*a*) uncooled and (*b*) cooled (projection of central axis of the fourth cooling hole shown in arrow)

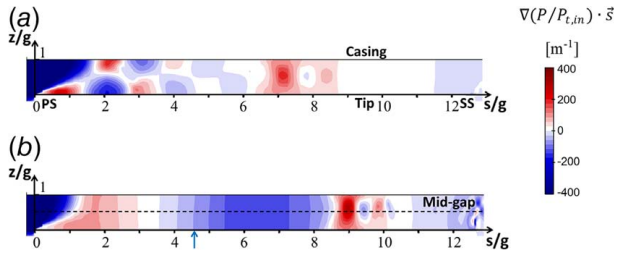

Fig. 21 Gradient of dimensionless static pressure along local OTL streamwise direction on cut plane 2 (location shown in Fig. 18(*a*)): (*a*) uncooled and (*b*) cooled (projection of central axis of the fourth cooling hole shown in arrow)

cut plane 2. Pressure at tip surface and mid-gap decreases before $s/g = 8.5$ and then increases in the shock train region. Pressure at mid-gap oscillates across each shock (at $s/g = 9$ and 10), but the fluctuation is not detected on the tip surface, because it is smeared out by the dissipation in wall boundary layer [49]. This behavior, as established for internal compressible flow in Ref. [47], once again substantiates that a shock train is formed within the tip gap.

One thing to note is that although the series of shocks for the cooled flat tip is directed normal to OTL flow coming from PS edge, as shown in Figs. 18(*b*) and 21(*b*), they are slightly different from the normal shock train that is encountered in internal compressible flow traditionally. Matsuo et al. [47] and Carroll and Dutton [48] reported that the core flow is decelerated to subsonic regime after each normal shock in a pocketed region, while the flow near boundary layer remains supersonic. In the present study, OTL flow is supersonic throughout the shock train, as shown in Fig. 19. One conjecture for this dilemma is the tip clearance in present study is much smaller than the duct height studied in Refs. [47,48], so the subsonic pocket in core flow is overshadowed by the supersonic outer flow near boundary layer. This argument is backed up by a recent study from Handa et al. [50]. They investigated supersonic flow in a microchannel having a rectangular cross section with a height of 0.5 mm, based on which the Reynolds number is 6200. Although the flow throughout the rectangular microchannel is supersonic, a cell structure relating to shock train is reported. In the present study, tip gap height is 0.675 mm and the corresponding Reynolds number based on a hydraulic diameter of twice the height is 9000 at the exit of tip clearance, which are close to those in Ref. [50].

Up to this point, connection between the shock train and the low Nusselt number stripe downstream of cooling injection from the fourth hole as remarked both experimentally and numerically in Sec. 4.1 can be readily clarified. Figure 23 graphs heat transfer coefficient and skin friction coefficient (C_f) on tip surface along local OTL flow direction on cut plane 2. Their trends are qualitatively

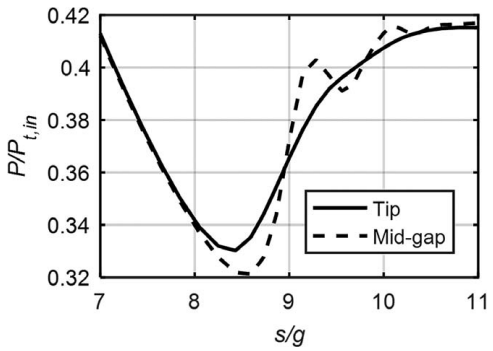

Fig. 22 Variation of dimensionless static pressure at tip surface and mid-gap along local OTL streamwise direction for the cooled case on cut plane 2 (location shown in Fig. 18(*a*))

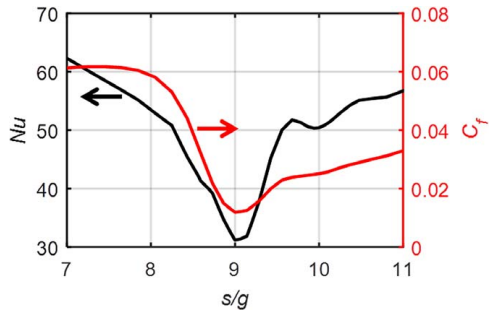

Fig. 23 Variation of Nusselt number and skin friction coefficient (C_f) along local OTL streamwise direction for the cooled case on cut plane 2 (location shown in Fig. 18(*a*))

the same. Minimum tip Nusselt number is spotted at $s/g = 9$, where skin friction is also the lowest. This is caused by the thickening of boundary layer due to the large adverse pressure gradient generated by the first shock in shock train. The second shock at $s/g = 10$ is much weaker and its influence on tip Nusselt number is inconspicuous. Aside from wall shear, which is largely set by the boundary layer thickness, the other mechanism that affects tip Nusselt number is turbulent mixing, which is correlated to local streamwise pressure gradient, as stated in Ref. [16]. After $s/g = 9$, turbulent viscosity within tip boundary layer rises due to the large adverse pressure gradient caused by the first shock in shock train. Hence, heat transfer is promoted evidently, although the increase of skin friction is limited.

5.3 Interaction Between Coolant and Overtip Leakage Flow. To better illustrate the interference phenomena between the cooling jet and OTL flow, flow quantities on plane 3 shown in Fig. 18(*a*) (which is cut through the central axis of the fourth hole) are contoured in Fig. 24. Spread of the coolant can be traced by the distribution of dimensionless total temperature, which is defined as $\theta = (T_{t,in} - T_t)/(T_{t,in} - T_{t,c})$. OTL-dominant region has a θ value close to 0 (hot), while coolant-dominant region has a θ value near 1 (cold). It is shown that coolant hits the casing directly after blowing from the hole on tip, which forms strong blockage to OTL flow entering from PS edge. As a result, pressure increases upstream of cooling injection and reduces sharply right downstream of the ejecting hole. Hence, OTL flow decelerates ahead of the cooling jet, as manifested by

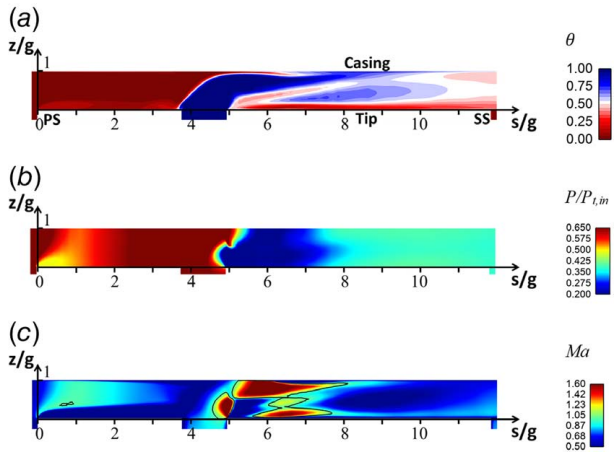

Fig. 24 Flow maps on cut plane 3 (cut through central axis of the fourth hole as shown in Fig. 18(*a*)): (*a*) dimensionless total temperature, (*b*) dimensionless static pressure, and (*c*) Mach number (contour of Mach=1 in black)

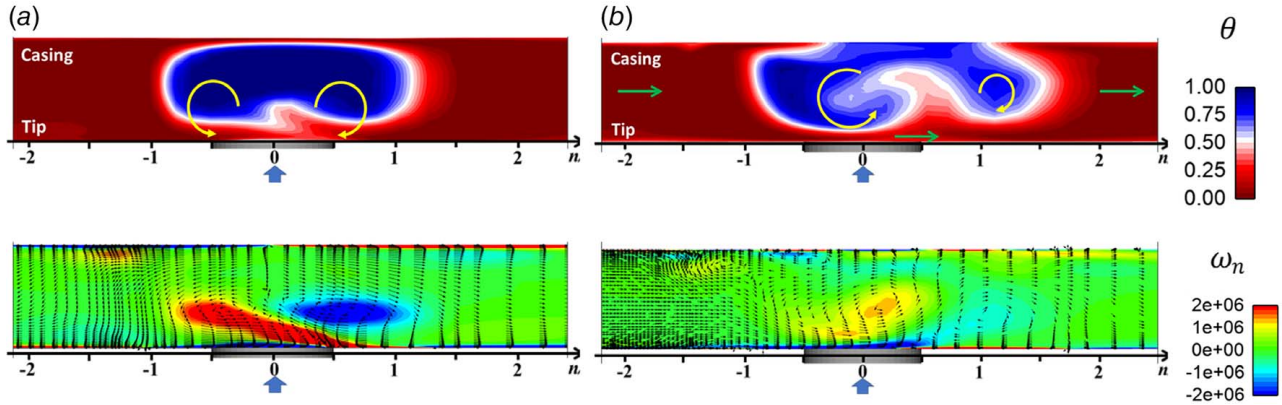

Fig. 25 Vortical flow structure of cooling injection: (*a*) cut plane 5 (located 1*D* downstream of the fourth hole as shown in Fig. 18(*a*) and (*b*) cut plane 6 (located 3*D* downstream of the fourth hole as shown in Fig. 18(*a*)

the low Mach number region in front of the jet. Right downstream cooling injection, tip flow accelerates rapidly to supersonic regime subject to the large favorable pressure gradient.

Another perspective to study the interaction between cooling injection and OTL flow is on the planes perpendicular to the streamwise direction of local OTL and coolant wake, which are cut tangentially to the camberline. Figure 25 plots dimensionless total temperature (θ) and normal vorticity (ω_n) on cut plane 5 and 6, which is situated 1*D* and 3*D* downstream of the central axis of the fourth hole (locations shown in Fig. 18(*a*)), as well as the projection of velocity vectors on each plane. Here, normal vorticity is defined as the dot product of vorticity and the unit normal vector of the plane, which physically represents the rotation the flow as projected on the plane, with counter-clockwise direction denoted as positive rotation. At 1*D* downstream of the hole (Fig. 25(*a*)), coolant core is situated near the casing and has a symmetric distribution, suggesting that cooling jet hits the casing after blowing from the hole and bifurcates. A CRVP appears near the bottom edge of the coolant core, due to the shearing between coolant and OTL that is wrapped around. The left leg of the CRVP is stronger than the right leg. At 3*D* downstream of the hole (Fig. 25(*b*)), coolant core becomes asymmetric, with the left branch much stronger than its right counterpart. As observed in the projection of velocity vectors, OTL flow tends to move from leading to trailing edge (positive n direction), subject to the mainstream pressure gradient in turbine passage. It circumvents the coolant core by flowing near the tip surface. In consequence, the left leg of the CRVP and the coolant core is strengthened, while the right let is weakened. Meanwhile, both legs incline to spread toward trailing edge rather than leading edge. These mechanisms are similar to that reported on a cooled squealer tip [27]. It should also be noted that on cut plane 1, 2, and 4 shown in Fig. 18(*a*), whose pitchwise coordinate is $n/D = -4.5$, -2.5, and 2.0, respectively, the local flow is entirely composed of tip leakage coming from PS edge, and the coolant has not spread to these planes.

Lastly, it is worth mentioning that the work in this paper is conducted in linear cascade with stationary casing. But the actual scenario in gas turbines is more complex because the blades are rotating. Previous work have used moving belts to simulate the effect of relative casing motion, and the results indicated that its effect on heat transfer coefficient of blade tips is small [51,52]. But in transonic cooled tips, interaction between tip shock wave and casing boundary layer, as well as the trajectory of cooling jet, whose core is situated near casing, is expected to be affected considerably by the relative casing motion, particularly at high moving speed. Thus, future work is suggested to include relative casing motion, with the support of experimental data. Nonetheless, interaction mechanism of shock wave, cooling jet and boundary layer on transonic blade tips is intrinsically complicated even in stationary linear cascade. Physical insights obtained in this paper provide a solid foundation to further elucidate the aerothermal physics of transonic turbine blade tips under rotating conditions.

6 Conclusions

Motivation for this paper comes from the scarcity of experimental data on transonic blade tip cooling, which are useful for tip designers, as well as the lack of physical insight on the interaction between shock wave and cooling in tip clearance, which is academically challenging. To the best of the authors' knowledge, this is the first of the kind heat transfer experimental data on transonic flat tip cooling, based on which cooling injection effect on overtip shock wave structure and heat transfer characteristics is elucidated for the first time in open literature.

Transient thermal measurements through infrared thermography on a transonic flat tip of a HPT blade with and without cooling injection were conducted in this paper. The linear turbine cascade has an exit Mach number of 0.95 and exit Reynolds number of 0.88×10^6. Five tip cooling holes are placed in rear part of blade where basedline OTL flow is supersonic. Experimental cases are also simulated by ANSYS FLUENT using three RANS models, whose reliability is validated against experimental data. The obtained heat transfer coefficients on cooled and uncooled tips show some consistent trends in experimental and numerical results. It is found that cooling injection changes tip heat transfer pattern dramatically. Tip Nusselt number is boosted significantly near PS (upstream of cooling injection), as well as in middle and aft portion of blade (around cooling holes). Remarkably, a narrow stripe of low Nusselt number is manifested downstream of cooling injection from the fourth hole. It is directed transverse to local OTL streamline which flows from PS to SS and extends to adjacent coolant wakes.

Analyses on aerothermal interaction physics are then performed by CFD to explain aforementioned heat transfer features. It is concluded that cooling injection changes OTL flow speed from supersonic to subsonic near PS (upstream of cooling injection) and in coolant wakes. It also influences tip aerodynamic field globally, i.e., in regions far away from ejection holes such as leading edge and trailing edge. Furthermore, cooling injection fundamentally alters overtip shock wave structure at the rear part of blade. Oblique shock waves across uncooled flat tip are supplanted by a shock train comprised two shocks normal to incoming OTL flow in the cooled tip. The shock train is located downstream of injection and between adjacent cooling holes, with the first shock much stronger than the second. Large adverse pressure gradient across the first shock in the shock train causes thickening of tip boundary layer. So skin friction on tip surfaces plunges, leading to the plummet of tip Nusselt number and thus, formation of the low

heat transfer stripe downstream the fourth cooling hole, as noted both experimentally and numerically.

Acknowledgment

Funding from Shanghai Science and Technology Committee (20YF1419100 and 21ZR1431800) and Shanghai Aerospace Science and Technology Innovation Foundation are acknowledged. The authors would also like to thank Professor Qiang Zhang, Professor Hua Ouyang, Dr. Shaopeng Lu, and Mr. Yongmin Gu at Shanghai Jiao Tong University for their kind support and help.

Conflict of Interest

There are no conflicts of interest.

Data Availability Statement

The datasets generated and supporting the findings of this article are obtainable from the corresponding author upon reasonable request. The authors attest that all data for this study are included in the paper. Data provided by a third party listed in Acknowledgment.

Nomenclature

Symbols

g = tip gap height (mm)
k = thermal conductivity (W/m-K)
n = normal coordinate to a surface
s = tangential coordinate to a surface
t = time (s)
x = axial coordinate (m)
y = circumferential coordinate (m)
z = radial coordinate (m)
D = diameter of cooling holes (mm)
P = pressure (Pa)
S = blade span (mm)
T = temperature (K)
U = velocity (m/s)
C_f = skin friction coefficient ($=\tau_w/(\rho_{in}U_{in}^2/2)$)
C_x = axial chord (mm)
T_{ad} = adiabatic wall temperature (K)
T_w = surface temperature (K)
q'' = heat flux (W/m^2)
R^2 = coefficient of correlation
h, HTC = heat transfer coefficient (W/m^2-K)

Greek Symbols

η = cooling effectiveness
θ = dimensionless total temperature ($=(T_{t,in}-T_t)/(T_{t,in}-T_{t,c})$)
μ = dynamic viscosity (Pa-s)
ρ = density (kg/m^3)
τ_w = wall shear stress (Pa)

Subscripts

c = coolant
e = exit of cascade
in = inlet of cascade
s = static
t = total

References

[1] Bogard, D. G., and Thole, K. A., 2006, "Gas Turbine Film Cooling," J. Propul. Power, **22**(2), pp. 249–270.
[2] Denton, J. D., 1993, "Loss Mechanisms in Turbomachines," ASME J. Turbomach., **115**(4), pp. 621–656.
[3] Azad, G. S., Han, J. C., Teng, S. Y., and Boyle, R. J., 2000, "Heat Transfer and Pressure Distributions on a Gas Turbine Blade Tip," ASME J. Turbomach., **122**(4), pp. 717–724.
[4] Newton, P. J., Lock, G. D., Krishnababu, S. K., Hodson, H. P., Dawes, W. N., Hannis, J., and Whitney, C., 2006, "Heat Transfer and Aerodynamics of Turbine Blade Tips in a Linear Cascade," ASME J. Turbomach., **128**(2), pp. 300–309.
[5] Bunker, R. S., Bailey, J. C., and Ameri, A. A., 2000, "Heat Transfer and Flow on the First-Stage Blade Tip of a Power Generation Gas Turbine: Part 1—Experimental Results," ASME J. Turbomach., **122**(2), pp. 263–271.
[6] Bunker, R. S., 2001, "A Review of Turbine Blade Tip Heat Transfer," Ann. NY Acad. Sci., **934**(1), pp. 64–79.
[7] Bunker, R. S., 2006, "Axial Turbine Blade Tips: Function, Design, and Durability," J. Propul. Power, **22**(2), pp. 271–285.
[8] Kwak, J. S., and Han, J. C., 2003, "Heat Transfer Coefficients and Film-Cooling Effectiveness on a Gas Turbine Blade Tip," ASME J. Heat Transfer-Trans. ASME, **125**(3), pp. 494–502.
[9] Ahn, J., Mhetras, S., and Han, J. C., 2005, "Film-Cooling Effectiveness on a Gas Turbine Blade Tip Using Pressure-Sensitive Paint," ASME J. Heat Transfer-Trans. ASME, **127**(5), pp. 521–530.
[10] Newton, P. J., Lock, G. D., Krishnababu, S. K., Hodson, H. P., Dawes, W. N., Hannis, J., and Whitney, C., 2009, "Aerothermal Investigations of Tip Leakage Flow in Axial Flow Turbines—Part 3: Tip Cooling," ASME J. Turbomach., **131**(1), p. 011008.
[11] Green, B. R., Barter, J. W., Haldeman, C. W., and Dunn, M. G., 2005, "Averaged and Time-Dependent Aerodynamics of a High Pressure Turbine Blade Tip Cavity and Stationary Shroud: Comparison of Computational and Experimental Results," ASME J. Turbomach., **127**(4), pp. 736–746.
[12] Didier, F., Dénos, R., and Arts, T., 2002, "Unsteady Rotor Heat Transfer in a Transonic Turbine Stage," ASME J. Turbomach., **124**(4), pp. 614–622.
[13] Arisi, A., Phillips, J., Ng, W. F., Xue, S., Moon, H. K., and Zhang, L., 2016, "An Experimental and Numerical Study on the Aerothermal Characteristics of a Ribbed Transonic Squealer-Tip Turbine Blade With Purge Flow," ASME J. Turbomach., **138**(10), p. 101007.
[14] Wheeler, A. P. S., Atkins, N. R., and He, L., 2011, "Turbine Blade Tip Heat Transfer in Low Speed and High Speed Flows," ASME J. Turbomach., **133**(4), p. 041025.
[15] Zhang, Q., O'Dowd, D. O., He, L., Oldfield, M. L. G., and Ligrani, P. M., 2011, "Transonic Turbine Blade Tip Aerothermal Performance With Different Tip Gaps—Part I: Tip Heat Transfer," ASME J. Turbomach., **133**(4), p. 041027.
[16] Zhang, Q., O'Dowd, D. O., He, L., Wheeler, A. P. S., Ligrani, P. M., and Cheong, B. C. Y., 2011, "Overtip Shock Wave Structure and Its Impact on Turbine Blade Tip Heat Transfer," ASME J. Turbomach., **133**(4), p. 041001.
[17] Zhang, Q., and He, L., 2011, "Overtip Choking and Its Implications on Turbine Blade-Tip Aerodynamic Performance," J. Propul. Power, **27**(5), pp. 1008–1014.
[18] Ma, H., Zhang, Q., He, L., Wang, Z., and Wang, L., 2017, "Cooling Injection Effect on a Transonic Squealer Tip—Part I: Experimental Heat Transfer Results and CFD Validation," ASME J. Eng. Gas Turbines Power, **139**(5), p. 052506.
[19] Saul, A. J., Ireland, P. T., Coull, J. D., Wong, T. H., Li, H., and Romero, E., 2019, "An Experimental Investigation of Adiabatic Film Cooling Effectiveness and Heat Transfer Coefficient on a Transonic Squealer Tip," ASME J. Turbomach., **141**(9), p. 091005.
[20] Vieira, J., Coull, J., Ireland, P., and Romero, E., 2020, "Aerothermal Effect of Cavity Welding Beads on a Transonic Squealer Tip," ASME Turbo Expo, Virtual, Online, Sept. 21–25.
[21] O'Dowd, D. O., Zhang, Q., He, L., Cheong, B. C. Y., and Tibbott, I., 2013, "Aerothermal Performance of a Cooled Winglet at Engine Representative Mach and Reynolds Numbers," ASME J. Turbomach., **135**(1), p. 011041.
[22] Lee, S. W., Jeong, J. S., and Hong, I. H., 2019, "Chord-Wise Repeated Thermal Load Change on Flat Tip of a Turbine Blade," Int. J. Heat Mass Transfer, **138**, pp. 1154–1165.
[23] Zhou, C., and Hodson, H. P., 2011, "The Tip Leakage Flow of an Unshrouded High Pressure Turbine Blade With Tip Cooling," ASME J. Turbomach., **133**(4), p. 041028.
[24] Volino, R. J., 2017, "Control of Tip Leakage in a High-Pressure Turbine Cascade Using Tip Blowing," ASME J. Turbomach., **139**(6), p. 061008.
[25] Wheeler, A. P. S., and Saleh, Z., 2013, "Effect of Cooling Injection on Transonic Tip Flows," J. Propul. Power, **29**(6), pp. 1374–1381.
[26] Wang, Z., Zhang, Q., Liu, Y., and He, L., 2015, "Impact of Cooling Injection on the Transonic Over-Tip Leakage Flow and Squealer Aerothermal Design Optimization," ASME J. Eng. Gas Turbines Power, **137**(6), p. 062603.
[27] Ma, H., Zhang, Q., He, L., Wang, Z., and Wang, L., 2017, "Cooling Injection Effect on a Transonic Squealer Tip—Part II: Analysis of Aerothermal Interaction Physics," ASME J. Eng. Gas Turbines Power, **139**(5), p. 052507.
[28] Krishnababu, S. K., Hodson, H. P., Booth, G. D., Lock, G. D., and Dawes, W. N., 2010, "Aerothermal Investigation of Tip Leakage Flow in a Film Cooled Industrial Turbine Rotor," ASME J. Turbomach., **132**(2), p. 021016.
[29] Naik, S., Georgakis, C., Hofer, T., and Lengani, D., 2012, "Heat Transfer and Film Cooling of Blade Tips and Endwalls," ASME J. Turbomach., **134**(4), p. 041004.
[30] Gao, J., Zheng, Q., Zhang, Z. Y., and Jiang, Y. T., 2014, "Aero-Thermal Performance Improvements of Unshrouded Turbines Through Management of Tip Leakage and Injection Flows," Energy, **69**, pp. 648–660.
[31] Wang, Y., Song, Y., Yu, J., and Chen, F., 2018, "Effect of Cooling Injection on the Leakage Flow of a Turbine Cascade With Honeycomb Tip," Appl. Therm. Eng., **133**, pp. 690–703.

[32] Niu, M., and Zang, S., 2011, "Experimental and Numerical Investigations of Tip Injection on Tip Clearance Flow in an Axial Turbine Cascade," Exp. Therm. Fluid Sci., **35**(6), pp. 1214–1222.
[33] Xue, S., Arisi, A., and Ng, W., 2015, "Experimental and Numerical Investigations of Shock-Film Cooling Interaction on a Turbine Blade With Fan-Shaped Cooling Holes," ASME J. Therm. Sci. Eng. Appl., **7**(4), p. 044502.
[34] Shiau, C.-C., Chowdhury, N. H., Han, J.-C., Mirzamoghadam, A. V., and Riahi, A., 2018, "Transonic Turbine-Vane Film Cooling with Showerhead Effect Using Pressure-Sensitive Paint Measurement Technique," J. Thermophys. Heat Transfer, **32**(3), pp. 637–647.
[35] Kodzwa, P. M., Jr., and Eaton, J. K., 2010, "Film Effectiveness Measurements on the Pressure Surface of a Transonic Airfoil," J. Propul. Power, **26**(4), pp. 837–847.
[36] Ligrani, P. M., Saumweber, C., Schulz, A., and Wittig, S., 2001, "Shock Wave–Film Cooling Interactions in Transonic Flows," ASME J. Turbomach., **123**(4), pp. 788–797.
[37] Zheng, R., Li, M., Wang, Z., and Zhang, Q., "Control of Blow-Down Wind Tunnel Using Combined Extended and Nonlinear Predictive Filters," Proc. ASME Paper Number GT2015-42908, American Society of Mechanical Engineers, p. V006T05A016.
[38] Xi, J., Zhang, Q., Li, M., and Wang, Z., "Advanced Flow Control for Supersonic Blowdown Wind Tunnel Using Extended Kalman Filter," Proc. ASME Paper Number GT2013-95281, American Society of Mechanical Engineers, p. V03CT14A025.
[39] Ma, H., Wang, Z., Wang, L., Zhang, Q., Yang, Z., and Bao, Y., 2016, "Ramp Heating in High-Speed Transient Thermal Measurement With Reduced Uncertainty," J. Propul. Power, **32**(5), pp. 1190–1198.
[40] Lu, S., Ma, H., Zhang, Q., and Teng, J., 2020, "Cutback Squealer Tip Trailing Edge Cooling Performance," Int. J. Heat Mass Transfer, **154**, p. 119632.
[41] Oldfield, M. L. G., 2008, "Impulse Response Processing of Transient Heat Transfer Gauge Signals," ASME J. Turbomach., **130**(2), p. 021023.
[42] Kays, W. M., Crawford, M. E., and Weigand, B., 2012, *Convective Heat and Mass Transfer*, Tata McGraw-Hill Education, New York.
[43] Mee, D., Chiu, H., and Ireland, P., 2002, "Techniques for Detailed Heat Transfer Measurements in Cold Supersonic Blowdown Tunnels Using Thermochromic Liquid Crystals," Int. J. Heat Mass Transfer, **45**(16), pp. 3287–3297.
[44] Arisi, A., Xue, S., Ng, W. F., Moon, H. K., and Zhang, L., 2015, "Numerical Investigation of Aerothermal Characteristics of the Blade Tip and Near-Tip Regions of a Transonic Turbine Blade," ASME J. Turbomach., **137**(9), p. 091002.
[45] Zhou, C., 2015, "Thermal Performance of Transonic Cooled Tips in a Turbine Cascade," J. Propul. Power, **31**(5), pp. 1268–1280.
[46] Shapiro, A. H., 1953, *The Dynamics and Thermodynamics of Compressible Fluid Flow*, John Wiley & Sons, New York.
[47] Matsuo, K., Miyazato, Y., and Kim, H. D., 1999, "Shock Train and Pseudo-Shock Phenomena in Internal Gas Flows," Prog. Aerosp. Sci., **35**(1), pp. 33–100.
[48] Carroll, B. F., and Dutton, J. C., 1992, "Multiple Normal Shock Wave/Turbulent Boundary-Layer Interactions," J. Propul. Power, **8**(2), pp. 441–448.
[49] Gnani, F., Zare-Behtash, H., and Kontis, K., 2016, "Pseudo-Shock Waves and Their Interactions in High-Speed Intakes," Prog. Aerosp. Sci., **82**, pp. 36–56.
[50] Handa, T., Kitahara, K., Matsuda, Y., and Egami, Y., 2019, "Peculiarities of Low-Reynolds-Number Supersonic Flows in Long Microchannel," Microfluid. Nanofluid., **23**(7), p. 88.
[51] Mayle, R. E., and Metzger, D. E., 1982, "Heat Transfer at the Tip of an Unshrouded Turbine Blade," Proceedings of the Seventh International Heat Transfer Conference, Munich, Germany, Sept. 6–10, pp. 87–92.
[52] Palafox, P., Oldfield, M. L. G., Ireland, P. T., Jones, T. V., and LaGraff, J. E., 2012, "Blade Tip Heat Transfer and Aerodynamics in a Large Scale Turbine Cascade With Moving Endwall," ASME J. Turbomach., **134**(2), p. 021020.